Impact of anomalous effects on the angular distribution of coherently scattered photons using Monte Carlo simulation

Wazir Muhammad[a,b] and Sang Hoon Lee[c]*

[a]Department of Physics, Kyungpook National University, 1370 Sankyuk-dong, Buk-gu, Daegu 702-701, Republic of Korea, [b]Department of Medical Physics, Institute of Nuclear Medicine, Oncology and Radiotherapy (INOR), Abbottabad, Pakistan, and [c]School of Energy Engineering, Kyungpook National University, 1370 Sankyuk-dong, Buk-gu, Daegu 702-701, Republic of Korea.
Correspondence e-mail: lee@knu.ac.kr

Comprehensive theoretical and experimental studies on the importance and application of anomalous scattering factors can be found in the literature. The aim of this study was to determine the role and impact of anomalous scattering factors on the Rayleigh scattering of photons, particularly within the regions around the elemental absorption edges, using Monte Carlo sampling techniques. In doing so, an improved version of the already established Monte Carlo techniques for Rayleigh scattering is proposed. The improved version is capable of using the available state-of-the-art anomalous scattering factors, and illustrates and highlights their role in calculating accurate coherent scattering amplitudes. A substantial increase in the forward scattering by the neutral atoms of germanium, caesium and lead, which is a maximum around the K edges due to the inclusion of anomalous scattering factors, was observed at all the energies that were examined. The results show that the angular distribution of coherent scattering of the photons depended upon the anomalous scattering factors. Serious errors could be produced when measuring the exact scattering amplitudes, particularly within the regions around the elemental absorption edges, by ignoring the effects of coherently scattered photons in the Monte Carlo sampling. Furthermore, the improved model provides some extra information on elemental K-edge energies by producing dips in the plots of the calculated normalized cumulative probability distribution function against the energy of the incident photons for all three elements. In conclusion, the use of complex atomic form factors has produced an improved and fairly good approximation which is in very good agreement with the corresponding experimental and scattering-matrix results.

1. Introduction

Accurate knowledge of the Rayleigh (elastic/coherent) scattering of photons from an isolated atom or ion, particularly near the photoeffect absorption edges, is the key to obtaining valuable information on the inner structure of a complex system. Accurate theoretical predictions for the Rayleigh scattering of photons is of great interest because of its potential applications in various fields, including structural chemistry and biology (Cianci et al., 2005), nuclear shielding, medical diagnostics etc. (Kissel et al., 1995; Roy et al., 1999, 1993).

In coherent scattering, a photon changes its direction only by negligible energy transfer to an effectively heavy primary target atom and retains the same energy after being scattered by a bound atomic electron (Kane et al., 1986; Pratt et al.,

1993). Mathematically, the differential cross section of coherent scattering can be written as (Kane et al., 1986; Persliden, 1983)

$$\frac{d\sigma_{coh}(Z, E, \theta)}{d\theta} = \frac{d\sigma_{th}(\theta)}{d\theta} f_0^{\,2}(Z, E, \theta)$$
$$= \frac{r_0^2}{2}(1 + \cos^2\theta)2\pi(\sin\theta)f_0^{\,2}(Z, \theta). \quad (1)$$

Here, $r_0 = 2.82 \times 10^{-13}$ cm is the classical electron radius, Z is the atomic number of the scattering element, E is the energy of the incident photon and $f_0(Z, \theta)$ is the atomic form factor (which represents the probability that the Z electrons of an atom take up the recoil momentum without absorbing any energy). In the literature, these form factors are often termed relativistic form factors (RFFs) or modified form factors (MFFs) (Hubbell & Overbo, 1979; Schaupp et al., 1983).

Electron binding corrections to the atomic form factors (AFFs) were first introduced by Franz in 1936 and the improved form factors are commonly known as MFFs (Kane *et al.*, 1986). However, equation (1) is approximately valid only for photons with energy well above the *K* absorption edges (Salvat *et al.*, 2011). In addition, it does not account for the effects at the elemental absorption edges (Cianci *et al.*, 2005). Furthermore, when the incident damped resonant X-rays have a frequency close to the natural frequency of the nucleus–electron dipole oscillator, the natural oscillation frequency of the dipole oscillator is affected by the energy of the incident X-ray (Sultana *et al.*, 2008). The atom is now acting as a forced oscillator under resonance conditions that cause changes in the amplitude and in the phase of the atomic scattering factor. By considering these factors, the differential cross section for the coherent scattering of unpolarized photons can be expressed as (Roy *et al.*, 1999; Salvat *et al.*, 2011)

$$\frac{d\sigma_{coh}(Z, E, \theta)}{d\theta} = = \frac{r_0^2}{2}(1 + \cos^2\theta)2\pi(\sin\theta)F^2(Z, E, \theta). \quad (1a)$$

The correction to equation (1) is called anomalous, and now $F(Z, E, \theta)$ is a complex quantity due to the damping effects. It can be written in terms of RFFs/MFFs plus the corrections for the anomalous scattering factors (ASFs) as shown in the following equation (Bergstrom *et al.*, 1997; Chantler, 2000; Roy *et al.*, 1999; Salvat *et al.*, 2011; Sultana *et al.*, 2008):

$$F^2(Z, E, \theta) = \left[f_0(Z, \theta) + f'(Z, E)\right]^2 + f''^2(Z, E). \quad (2)$$

Here, f_0 is the RFF/MFF which accounts for the effect of interfering scattering amplitudes across the atoms. f' and f'' are the real and imaginary parts of the complex scattering amplitude of the ASFs, respectively. These are also known as the dispersion corrections to the form factors (Chantler, 2000; Tartari *et al.*, 2002).

The complex form of $F(Z, E, \theta)$ is helpful in specifying the refractive indices, permittivities, scattering/attenuation coefficients and some other critical properties for optical devices (*i.e.*, mirrors, lenses, filters and coatings), while at higher photon energies it becomes accessible to theoretical predictions (Chantler, 2000). The role of anomalous scattering in structural chemistry and biology, and protein crystallography, has been highlighted by Cianci *et al.* (2005) and Sultana *et al.* (2008), respectively. However, the RFF/MFF approximation fails to predict any of the effects related to atomic structure, such as virtual excitation and ionization of atomic electrons for photon energies close to the absorption edges (Kissel *et al.*, 1995); furthermore, it is a high-photon-energy and small-momentum-transfer approximation. The RFF/MFF approximation can provide good predictions for small-angle differential and angle-integrated cross sections only for photon energies that are above the *K*-shell photoeffect threshold of an atom (Kissel *et al.*, 1995; Roy *et al.*, 1999). The RFF/MFF approximation does not perform well at photon energies below and within the inner shell photoeffect threshold or with large angles for photon energies well above the *K*-shell photoeffect threshold for high-*Z* elements. In contrast, the MFF/RFF + ASF approximation (*i.e.*, using complex atomic

form factors) provides an accurate and efficient way to predict Rayleigh scattering cross sections below, near and above the *K*-shell photoeffect threshold for all angles (Kissel *et al.*, 1995; Roy *et al.*, 1999). Pratt *et al.* (1993) recommended the MFF + ASF scheme as a relatively simple and accurate scheme for estimating elastic scattering amplitudes and cross sections.

Extensive and complete tabulations of f_0 (*i.e.*, RFFs and MFFs) for all neutral atoms in the periodic table were published during the last quarter of the 20th century (Hubbell & Overbo, 1979; Schaupp *et al.*, 1983). These are traditionally tabulated as a function of the variable $v = \lambda^{-1}[\sin(\theta/2)]$ [where λ (Å) is the incident photon wavelength], with units of inverse length (Å^{-1}). Additionally, anomalous scattering can be derived classically by treating the scattering interaction as a pair of coupled oscillators (*i.e.*, the electric component of the incident X-ray wave and a bound electron of the scattering atom) (Sultana *et al.*, 2008). ASFs have been computed by Cullen (1989) using the relativistic dispersion relation previously described by Pratt *et al.* (1993) and contain information about the edge structure of atoms, where f'' includes a Rydberg series of resonances, and ASFs are useful in identifying the composition of the scattering systems (Bergstrom *et al.*, 1997). An extensive tabulation of ASFs as a function of the energy of the photons for all atomic numbers can be found in the literature (Cromer, 1983; Cromer & Liberman, 1970; Henke *et al.*, 1993, 1981). The computer program *FPRIME* evaluates these ASFs for arbitrary atomic number and photon energy in the range 1–70 keV, while another set of ASFs based on the interpolation and extrapolation of experimentally measured photoeffect cross sections is available for all atomic numbers and photon energies from ~0.03 to 30 keV (Cromer, 1983; Henke *et al.*, 1993, 1981). Data for the ASFs are also easily accessible online at http://henke.lbl.gov/optical_constants/asf.html for all 92 elements from 0.01 to 30 keV with points added 0.1 eV above and below the 'sharp' absorption edges.

In the literature, one can find extensive theoretical calculations for the Rayleigh scattering of photons. Some of these are publicly available and some are distributed for specific users in the form of data libraries (*i.e.* EPDL97, the RTAB database *etc.*). EPDL97 (Evaluated Photon Data Library, 1997 version) (Cullen *et al.*, 1997) was adopted as the source of photon interaction data for the official United States ENDF system, first as part of ENDF/B-VI, and currently as ENDF/B-VII.1 (Chadwick *et al.*, 2011). It contains evaluated nuclear data files, total cross sections, AFFs and ASFs. The dynamic range for the photon energies is from 1 eV to 100 GeV for elements having $Z = 1$–100. EPDL97 uses non-relativistic form factors (NFFs) and ASFs from Hubbell *et al.* (1975) and Cullen (1989), respectively. With the numerical integration method, the total Rayleigh cross sections are derived from the Thomson scattering, AFFs and ASFs. The method uses different estimations for such calculations but one cannot find the details of these estimations. EPDL97 is extensively used in Monte Carlo (MC) simulation packages. A set of photon Rayleigh scattering cross sections has also been included in RTAB (Kissel, 2000) by following various calculation methods

using AFFs and ASFs. The differential cross sections tabulated in RTAB are based on NFFs from Hubbell *et al.*, RFFs, MFFs, numerical S-matrix calculations by Kissel and Pratt, and MFFs + ASFs. However, to the best of our knowledge, EPDL97 was the first to include ASFs in a major data library comprehensively covering the entire periodic table, $Z = 1$–100. The RTAB database has two sets of cross sections based on S-matrix tabulations. One set of data takes into account only the Rayleigh scattering amplitude, while other takes into account the Thomson scattering amplitudes along with the Rayleigh scattering amplitude. In contrast to EPDL97, RTAB is still waiting to be exploited in general-purpose MC codes (Batič *et al.*, 2012).

MC simulation methods for the angular distribution of coherently scattered photons have been shown to be the most appropriate tools (Muhammad & Lee, 2013). A number of MC-based computer codes are currently available for photon transport with coherent scattering as their integral part (*i.e.*, MCNP, EGSnrc, PENELOPE, GEANT4 *etc.*). The algorithms for Rayleigh scattering of photons are an integral part of these MC codes. Most of these algorithms are based on the form-factor approximation. The other amplitudes usually involved in the Rayleigh scattering of photons do not appear to be taken into account by these codes, apart from the implicitly included Thomson scattering while calculating the total cross sections with codes using EPDL97 (Batič *et al.*, 2012). We discuss below the current status of MC sampling techniques adopted by these well known codes for coherent scattering.

MCNP is one of the best known and oldest general-purpose Monte Carlo *N*–particle codes that can be used for detailed simulation of photon transport (Demarco *et al.*, 2002; X-5 Mote Carlo Team, 2003). Primarily, equation (1*a*) has been used for MC modeling of the coherent scattering of photons. However, ASFs are approximated to be zero by assuming that the ASFs are isotropic and angle independent. In practice, the approximation reduces equation (1*a*) to equation (1) for further processing. Furthermore, inside the MCNP code, the electron-binding effects associated with Rayleigh scattering are handled by the coherent RFFs (Demarco *et al.*, 2002).

EGSnrc is the most widely used general-purpose Monte Carlo radiation (*i.e.*, electron–photon) transport package. The dynamic range is between 1 keV to several tens of GeV for elements ($Z = 1$–100), arbitrary compounds and mixtures (Kawrakow *et al.*, 2010). The AFFs from Hubbel & Overbo (1979) are used inside EGSnrc for MC simulation of coherent scattering of photons while ignoring the ASFs (Kawrakow *et al.*, 2010).

PENELOPE is another Monte Carlo simulation code for coupled electron–photon transport for arbitrary materials and complex quadric geometries. Photon interactions (Rayleigh scattering, Compton scattering, photoelectric effect and electron–positron pair production) and positron annihilation can be simulated through this MC package. Although the total atomic cross sections for elements used in PENELOPE are from EPDL (Cullen, 1997; Cullen *et al.*, 1997) and are calculated from the differential cross section shown in equation (2) (*i.e.*, including the ASFs), when calculating the differential cross section for compound/composite molecules, the ASFs are ignored. However, for the MC sampling techniques adopted inside PENELOPE for coherent scattering events, ASFs are ignored with the assumption that these are independent of the photon scattering angle (Salvat *et al.*, 2011).

The same approximation is used in GEANT4 while simulating coherent scattering events (Batič *et al.*, 2012). On the other hand, the angle-independent assumption for the ASFs fails for finite angles at photon energies well above the *K* threshold for high-*Z* elements (Kissel *et al.*, 1995). In addition, Bergstrom *et al.* (1997) presented a simple formula to calculate the angle dependence of the ASFs in the elastic photon–atom scattering amplitude at an arbitrary angle.

TART12 by Dermott E. Cullen is also a coupled neutron–photon, three-dimensional, combinatorial geometry, time-dependent MC radiation transport code (Cullen, 2012). The earlier versions of TART include TART 2005, TART 2002, TART98, TART97, TART96, TART9 and TART94 (Cullen, 1995, 1997, 1998, 2000, 2003, 2012). The earlier versions state that ASFs have less of an important effect on angular distributions near the photoelectric edges and are therefore ignored (Cullen, 1995). An improved treatment for photon coherent scattering was included in TART98 (Cullen, 1998), but we were not able to find the details of these improvements in the literature. However, from private communications in 2012 with Dermott E. Cullen, we found that ASFs have been included for sampling of coherently scattered photons in the TART MC package since 1997, which shows its importance in the angular distribution of coherently scattered photons, particularly within the regions around the elemental absorption edges.

The above discussion clarifies the importance of coherent scattering by bound atomic electrons with low energy X-rays and soft γ-rays, particularly within the regions around the elemental absorption edges. Therefore, much effort has been devoted to calculating accurate theoretical values for RFFs, MFFs, ASFs and the scattering cross sections using these factors. Previous studies on the MFF/RFF + ASF scheme also highlighted the importance of ASFs in calculating the

Table 1
List of energies used for the Monte Carlo simulations with corresponding nearby edge energies for each element studied.

Germanium (Ge, $Z = 32$)		Caesium (Cs, $Z = 55$)		Lead (Pb, $Z = 82$)	
Energy for MC simulation (keV)	Nearby edge energy (keV)	Energy for MC simulation (keV)	Nearby edge energy (keV)	Energy for MC simulation (keV)	Nearby edge energy (keV)
$E1 = 1.2167$	L_{III}: 1.2167	$E1 = 5.007$	L_{III}: 5.0119	$E1 = 2.48$	M_5: 2.484
$E2 = 1.2304$	L_{II}: 1.2478	$E2 = 5.301$	L_{II}: 5.3594	$E2 = 2.58$	M_4: 2.5856
$E3 = 10.966$	K: 11.1031	$E3 = 5.695$	L_{I}: 5.7143	$E3 = 13.1$	L_{III}: 13.0352
$E4 = 11.103$	K: 11.1031	$E4 = 35.83$	K: 35.985	$E4 = 15.1$	L_{II}: 15.2
				$E5 = 15.6$	L_{I}: 15.8608
				$E6 = 88.6$	K: 88.0045

Table 2
Maximum (max), mean and standard deviation (SD) of the % differences between normalized values of $A_{\mathrm{MFF}}(Z, v_i^2)$ and $A_{\mathrm{MFF+ASF}}(Z, v_i^2)$ for v_i^2 calculated on the basis of the MFF and MFF/RFF + ASF schemes, respectively.

Values are given for: germanium (Ge, $Z = 32$) at energies $E1 = 1.2167$ keV, $E2 = 1.2304$ keV, $E3 = 10.966$ keV and $E4 = 11.103$ keV; caesium (Cs, $Z = 55$) at energies $E1 = 5.007$ keV, $E2 = 5.301$ keV, $E3 = 5.695$ keV and $E4 = 35.83$ keV; and lead (Pb, $Z = 82$) at energies $E1 = 2.48$ keV, $E2 = 2.58$ keV, $E3 = 13.1$ keV, $E4 = 15.1$ keV, $E5 = 15.6$ keV and $E6 = 88.6$ keV.

	Germanium (Ge, $Z = 32$)				Caesium (Cs, $Z = 55$)				Lead (Pb, $Z = 82$)					
	E1	E2	E3	E4	E1	E2	E3	E4	E1	E2	E3	E4	E5	E6
Max (%)	12.54	7.36	29.57	28.76	22.25	13.37	5.54	42.62	17.61	7.75	25.00	17.65	12.29	39.17
Mean (%)	7.47	4.35	20.44	19.69	13.19	7.88	3.03	30.95	11.24	4.63	17.58	11.58	7.91	22.68
SD (%)	4.97	2.91	9.94	9.71	7.44	4.44	1.88	13.34	6.74	3.06	9.00	6.29	4.39	14.43

coherent scattering cross sections. The currently available widely used MC packages use RFFs/MFFs while ignoring ASFs for the sampling of coherent scattering of photons by arguing that these are angle independent and isotropic, except

Figure 1
Mean, standard deviation and maximum values of the % differences between normalized values of $A_{\mathrm{MFF/RFF}}(Z, v_i^2)$ and $A_{\mathrm{MFF/RFF+ASF}}(Z, v_i^2)$ for v_i^2 calculated on the basis of the MFF/RFF and MFF/RFF + ASF schemes, respectively. (a) Germanium (Ge, $Z = 32$), energies for $A_{\mathrm{MFF/RFF+ASF}}(Z, v_i^2)$: $E1 = 1.2167$ keV, $E2 = 1.2304$ keV, $E3 = 10.966$ keV and $E4 = 11.103$ keV. (b) Caesium (Cs, $Z = 55$), energies for $A_{\mathrm{MFF/RFF+ASF}}(Z, v_i^2)$: $E1 = 5.007$ keV, $E2 = 5.301$ keV, $E3 = 5.695$ keV and $E4 = 35.83$ keV. (c) Lead (Pb, $Z = 82$), energies for $A_{\mathrm{MFF/RFF+ASF}}(Z, v_i^2)$: $E1 = 2.48$ keV, $E2 = 2.58$ keV, $E3 = 13.1$ keV, $E4 = 15.1$ keV, $E5 = 15.6$ keV and $E6 = 88.6$ keV.

for TART, which has been using these factors since 1997. However, the role of the ASFs in calculating the coherent scattering cross section, as suggested by various research groups (Bergstrom et al., 1997; Kissel et al., 1995), including the use of these factors by TART, makes the argument regarding angle independence and the isotropic nature of ASFs very weak. As a result, the use of these codes might not be 100% beneficial to areas where the use of coherent scattering is the primary concern unless the correction for ASFs is not implied. Therefore, the present study was designed to illustrate and highlight the role of ASFs on the angular distribution of coherently scattered photons particularly within the regions around the elemental absorption edges using the available state-of-the-art theoretical knowledge on coherent scattering.
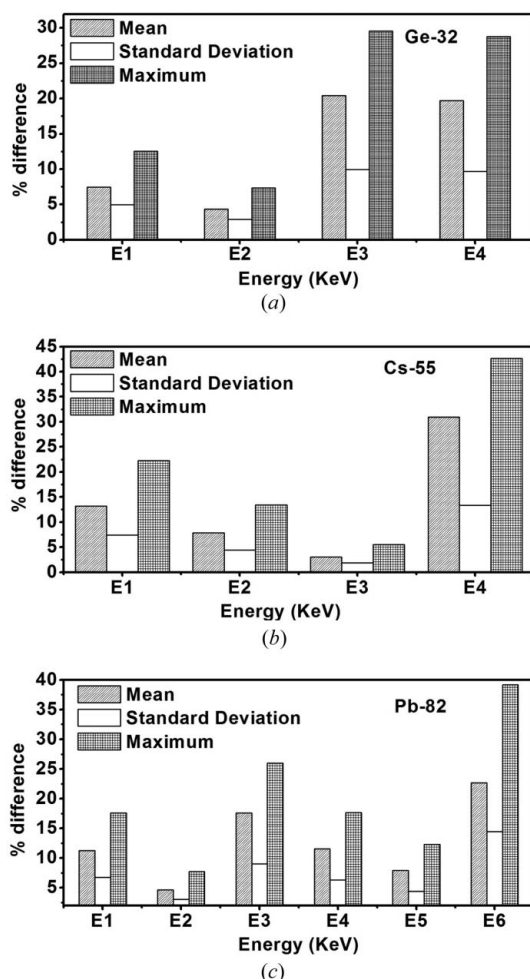
2. Monte Carlo simulation

An improved model for the implementation of ASFs in the MC sampling of coherently scattered photons based on the rejection technique is proposed. The improved model is implemented using techniques already developed over the past several decades for the coherent scattering of photons. According to these established sampling techniques, the probability of coherently scattered photons being scattered into the polar angle interval $d\theta$ around θ is given by

$$p(\theta)\,\mathrm{d}\theta = \frac{\mathrm{d}\sigma_{\mathrm{coh}}(Z, E, \theta)\,\mathrm{d}\theta}{\sigma_{\mathrm{coh}}(E, \theta)}$$
$$= \frac{r_0^2}{2}\frac{(1 + \cos^2\theta)F^2(Z, E, v)2\pi(\sin\theta)\,\mathrm{d}\theta}{\sigma_{\mathrm{coh}}(E, \theta)}. \quad (3)$$

Here, σ_{coh} is the total coherent cross section (Kawrakow et al., 2010; Muhammad & Lee, 2013; Persliden, 1983; X-5 Monte Carlo Team, 2003). Let us suppose $\mu = \cos\theta$ and $\alpha = E/m_0c^2$ (where m_0c^2 is the electron rest mass energy), and rewrite equations (1a) and (3) (Carter & Cashwell, 1975; Muhammad & Lee, 2013) as

$$\mathrm{d}\sigma_{\mathrm{coh}}(Z, E, \mu)\,\mathrm{d}\mu = \pi r_0^2(1 + \mu^2)F^2(Z, E, v)\,\mathrm{d}\mu, \quad (4)$$

$$p(\mu)\,\mathrm{d}\mu = \frac{\mathrm{d}\sigma_{\mathrm{coh}}(Z, \alpha, \mu)\,\mathrm{d}\mu}{\sigma_{\mathrm{coh}}(Z, E)}. \quad (5)$$

From the relation $v = \sin(\theta/2)/\lambda$ the following equation can be easily established with a trigonometric relation [i.e.,
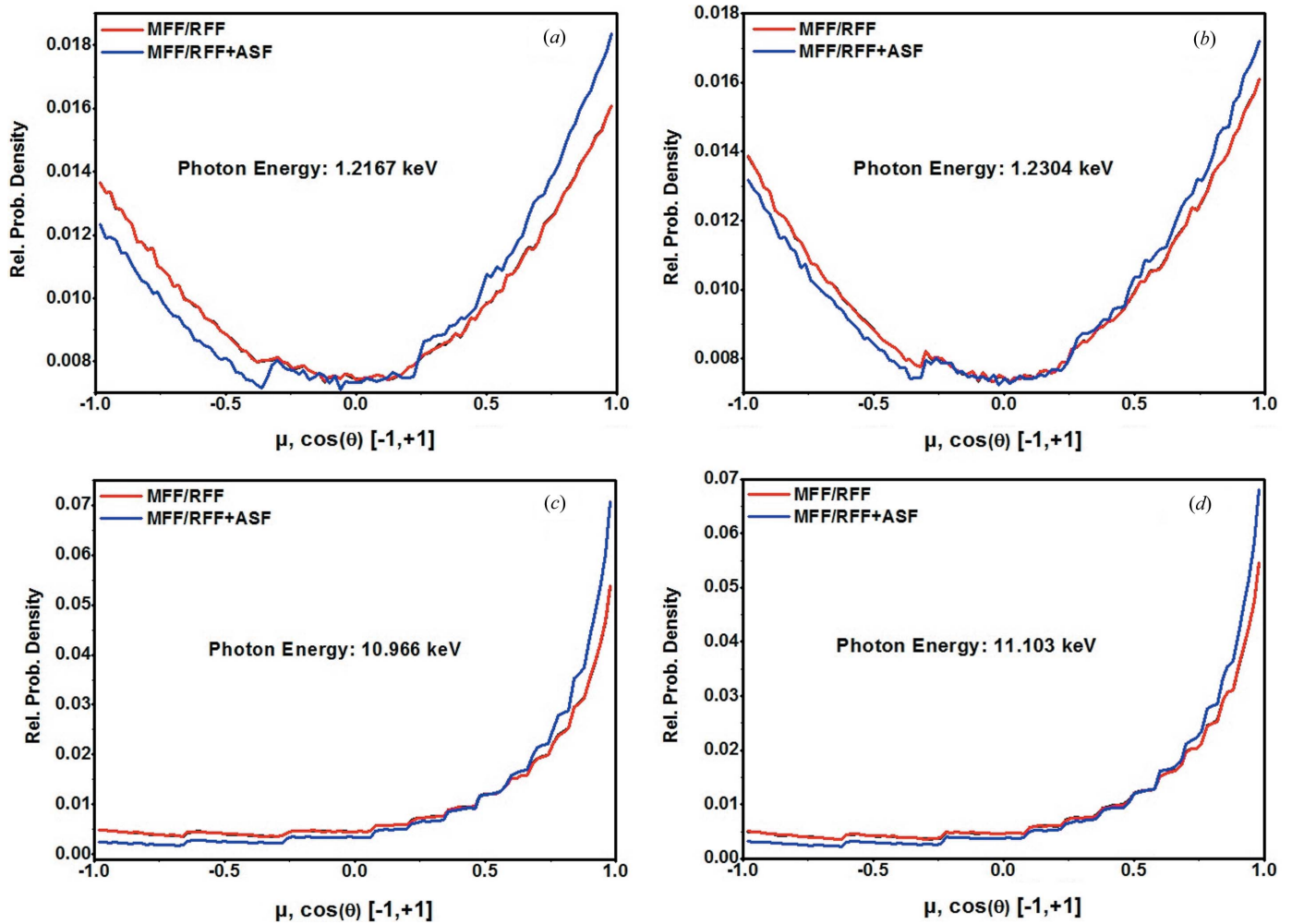
Figure 2
Angular distribution of the coherently scattered photons sampled on the basis of the MFF/RFF and MFF/RFF + ASF schemes for a source of 1 000 000 photons after being scattered by germanium (Ge, Z = 32) at energies (a) $E1$ = 1.2167 keV, (b) $E2$ = 1.2304 keV, (c) $E3$ = 10.966 keV and (d) $E4$ = 11.103 keV.

$\sin^2(\theta/2) = (1/2)(1 - \cos\theta)]$ and the energy and wavelength relation.

$$v^2 = (k\alpha)^2(1 - \mu), \quad 0 \le v^2 \le \overline{v}^2. \quad (6)$$

Here, $k = 10^{-8}m_0c/h(2)^{1/2} = 29.1445$ cm^{-1} and $\overline{v}^2 = 2(k\alpha)^2$ corresponds to the $v_{\max}$ (Muhammad & Lee, 2013; X-5 Monte Carlo Team, 2003). Equation (4) can be rewritten as

$$p(v^2)\,dv^2 = p_{coh}(\mu)\left|\frac{d\mu}{dv^2}\right|dv^2. \quad (7)$$

From equation (6), the relations $\mu = 1 - [v^2/(k\alpha)^2]$ and $d\mu/dv^2 = -1/(k\alpha)^2$ can be easily extracted. Equation (7) becomes

$$p(v^2)\,dv^2 = \frac{d\sigma_{coh}(Z, \alpha, \mu)}{\sigma_{coh}(Z, E)}\left|\frac{d\mu}{dv^2}\right|dv^2$$
$$= \frac{d\sigma_{coh}(Z, \alpha, \mu)}{\sigma_{coh}(Z, \alpha)}\left|-1/(k\alpha)^2\right|dv^2. \quad (8)$$

The combination of equations (4) and (8) yields

$$p(v^2)\,dv^2 = \frac{\pi r_0^2 z^2}{(k\alpha)^2\sigma_{coh}(Z, E)}\left(1 + \mu^2\right)\frac{F^2(Z, E, v)\,dv^2}{z^2}. \quad (9)$$

Now, by introducing the following relations for arbitrary v^2, equations (10) and (11) are as follows:

$$A(Z, E, v^2) = \int_0^{v^2} F^2(Z, E, v)Z^{-2}\,dv^2, \quad (10)$$

$$\overline{A}(Z, E, \overline{v}^2) = \int_0^{\overline{v}^2} F^2(Z, E, v)Z^{-2}\,dv^2. \quad (11)$$

These can be easily calculated by numerical integration; hence, equation (9) becomes

$$p(v^2)\,dv^2 = \frac{2\pi r_0^2 z^2 A(Z, E, \overline{v}^2)}{(k\alpha)^2\sigma_{coh}(Z, E)}\left(\frac{1 + \mu^2}{2}\right)\frac{F^2(Z, E, v)\,dv^2 z^{-2}}{A(Z, E, \overline{v}^2)}. \quad (12)$$

Let us consider $Q(v^2) = F^2(Z, E, v)z^{-2}/\overline{A}(Z, E, \overline{v}^2)$, $G(v^2) = (1 + \mu^2)/2$ and $C_0(Z, E) = 4\pi r_0^2 z^2 \overline{A}(Z, E, \overline{v}^2)/\sigma_{coh}(Z, E)\overline{v}^2$; then equation (12) can be written as

$$p(v^2)\,dv^2 = C_0(Z, E)G(v^2)Q(v^2)\,dv^2.$$

The probability distribution function (PDF) of the angular deflection μ can also be written as (Muhammad & Lee, 2013; Salvat *et al.*, 2011)

$$p_{coh}(\mu) = G(v^2)Q(v^2). \tag{13}$$

To assign v^2 with density $Q(v^2)$, a random number $\xi = \int_0^{v^2} Q(v^2)\,dv^2 = A(Z, E, v^2)/\overline{A}(Z, E, \overline{v}^2)$ on (0 to 1) can therefore be used and the value of v^2 is accepted as the probability as follows (Carter & Cashwell, 1975; Kawrakow *et al.*, 2010; Muhammad & Lee, 2013; Persliden, 1983):

$$G(v^2) = \frac{1 + \mu^2}{2} \leq 1. \tag{14}$$

The required values of f' and f'' for a specific energy are determined by linear interpolation using their tabulated values against energy. These values are combined with the tabulated values of the MFFs/RFFs against v to calculate $F(Z, E, \mu)$ through equation (2). The integrated values of $F^2(Z, E, v_i^2)$ against v^2 for $v_i^2 = v_1^2, \ldots, \overline{v}^2$ are calculated by the function that is included for the calculation of $A_{MFF/RFF+ASF}(Z, E, v_i^2)$. Now, both f' and f'' are approximated as zero if the anomalous effects were not considered and the same procedure is followed for the calculation of $A_{MFF/RFF}(Z, v_i^2)$. These steps are followed when running each code for the MC simulation of the coherent scattering of photons. The study was performed for germanium (Ge, $Z = 32$), caesium (Cs, $Z = 55$), tantalum (Ta, $Z = 73$) and lead (Pb, $Z = 82$) for energies of photons around their characteristic

Figure 3
(*a*) Comparison of the forward coherent scattering peaks for germanium (Ge, $Z = 32$). (*b*) % difference between the peaks calculated on the basis of the MFF/RFF and MFF/RFF + ASF schemes for germanium. Energies: E1 = 1.2167 keV, E2 = 1.2304 keV, E3 = 10.966 keV and E4 = 11.103 keV.

absorption edges, since the largest changes in the differential cross section due to the ASFs occur around these edges. The energies around the elemental absorption edges for which the values of f' and f'' were available were used for the MC simulation. These energies, with the corresponding nearby absorption edges for each element studied, are listed in Table 1.

First, the normalized values of $A_{MFF/RFF+ASF}(Z, v_i^2)$ for the energies listed in Table 1 and $A_{MFF/RFF}(Z, v_i^2)$ based on the MFF/RFF + ASF and MFF/RFF schemes, respectively, were introduced to circumvent large differences between them for each element studied. Each data set for these values is normalized by their maximum value. The % differences between $A_{MFF/RFF}(Z, v_i^2)$ and $A_{MFF/RFF+ASF}(Z, v_i^2)$ based on the MFF/RFF and MFF/RFF + ASF schemes, respectively, were calculated using

$$\% \text{ difference} =$$
$$\frac{A_{MFF/RFF}(Z, v_i^2) - A_{MFF/RFF+ASF}(Z, v_i^2)}{\left[A_{MFF/RFF}(Z, v_i^2) + A_{MFF/RFF+ASF}(Z, v_i^2)\right]/2} \times 100. \tag{15}$$

The maximum, mean and standard deviation (SD) of the % differences between the normalized values of $A_{MFF/RFF}(Z, v_i^2)$ and $A_{MFF/RFF+ASF}(Z, v_i^2)$ for Ge-32, Cs-55 and Pb-82 at the listed energies were also calculated. To study the impact of the anomalous scattering effects on the Monte Carlo sampling for coherently scattered photons, the first PDF was constructed through $A_{MFF/RFF}(Z, v_i^2)$ for $v_i^2 = v_1^2, \ldots, \overline{v}^2$ and then through $A_{MFF/RFF+ASF}(Z, v_i^2)$ for $v_i^2 = v_1^2, \ldots, \overline{v}^2$ using the MC techniques described above for the energies given for each element in Table 1.

The MC sampled relative probability density curves of the photon angular distribution μ can be used to calculate the cumulative probability distribution function (CDF) for the coherently scattered photons. The CDF can be calculated as

$$CDF_{coh}(\mu) = \int_{-1}^{+1} p_{coh}(\mu)\,d\mu. \tag{16}$$

To calculate the CDFs and normalized cumulative probability distribution functions (nCDFs), the MC techniques described above were used to sample the relative probability density curves for the elements listed in Table 1. The curves were sampled using the MFF/RFF and MFF/RFF + ASF schemes for each element. Sampling with both the MFF/RFF and MFF/RFF + ASF schemes was performed with energies from 1 to 17 keV, 42 keV and 808 keV for Ge-32, Cs-55 and Pb-82, respectively. The CDFs for the coherent scattering of photons by the neutral atoms Ge-32, Cs-55 and Pb-82 as a function of the energy of the incident photon were calculated by applying numerical integration to each sampled curve. Separate CDF value sets based on the MFF/RFF and MFF/RFF + ASF schemes were obtained for Ge-32, Cs-55 and Pb-82. The nCDFs, defined as the ratio of the CDF at a given energy of the photon to the CDF, correspond to the normalization energy (*i.e.*, its maximum value at the specified energy range) for both the MFF/RFF and MFF/RFF + ASF schemes and were calculated for each element.
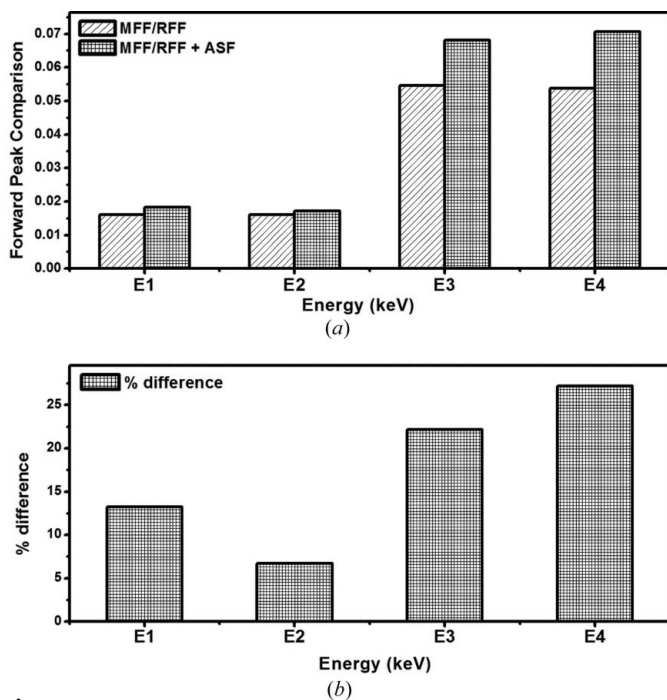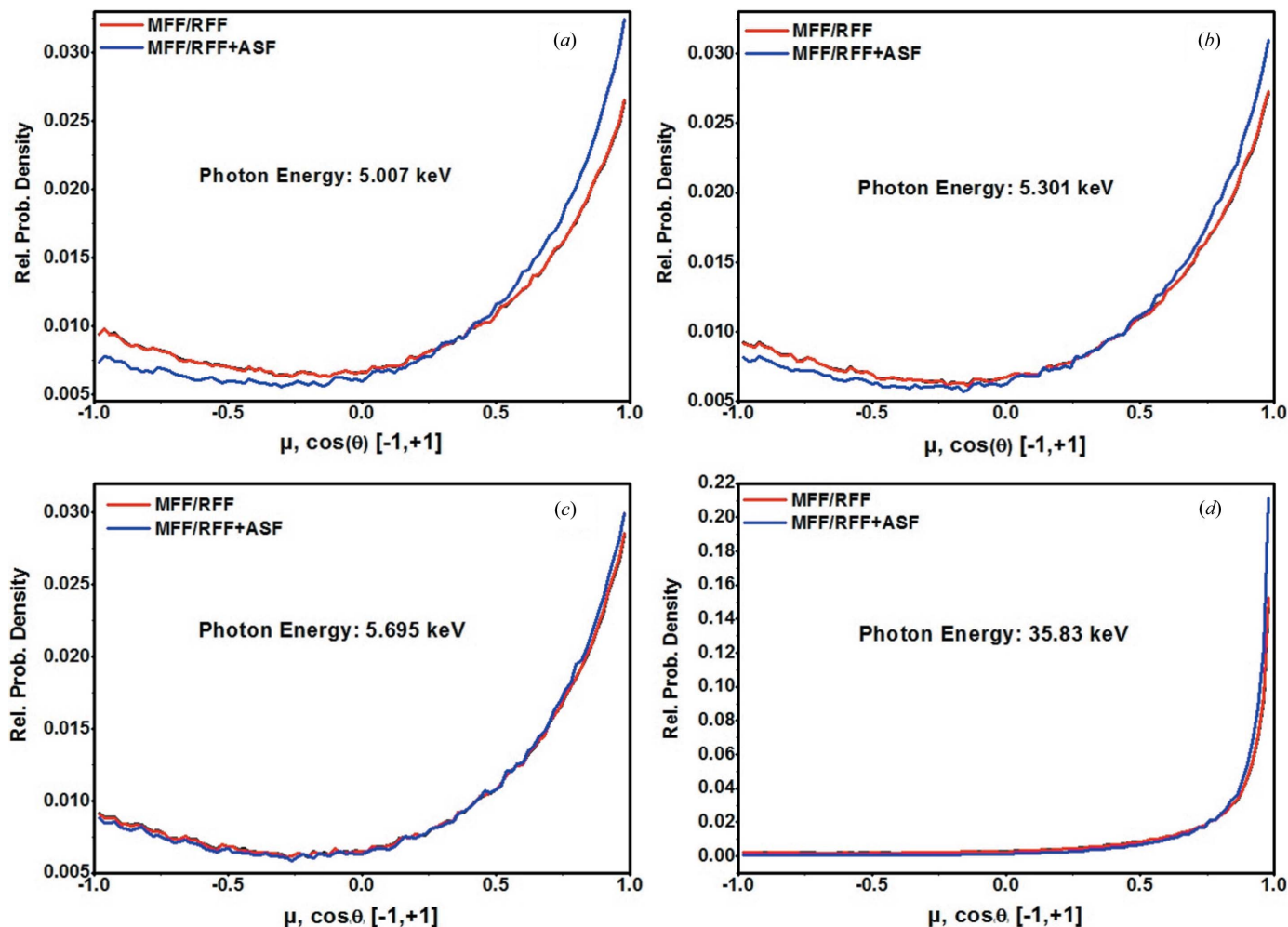
Figure 4
Angular distribution of the coherently scattered photons sampled on the basis of the MFF/RFF and MFF/RFF + ASF schemes for a source of 1 000 000 photons after being scattered by caesium (Cs, $Z = 55$) at energies (*a*) $E1 = 5.007$ keV, (*b*) $E2 = 5.301$ keV, (*c*) $E3 = 5.695$ keV and (*d*) $E4 = 35.83$ keV.

To compare the results with experimental, scattering-matrix (SM) and theoretical (*i.e.*, using only the MFF and RFF approximations) results, data for the differential cross section (DCS) for a neutral atom of tantalum (Ta, $Z = 73$) at a photon energy of 59.54 keV, which is close to its K edge (*i.e.*, 67.4164 keV), were taken from Pratt *et al.* (1993). The data were normalized by the total cross section at 59.54 keV. The normalized DCS (nDCS) was compared with the corresponding simulated results from the current MC code.

3. Results and discussion

The maximum, mean and SD of the % differences between the normalized values of $A_{\mathrm{MFF/RFF}}(Z, v_i^2)$ and $A_{\mathrm{MFF+ASF}}(Z, v_i^2)$ for Ge-32, Cs-55 and Pb-82 at the energies listed in Table 1 are summarized in Table 2. These values are also shown in Fig. 1. A maximum % difference of 29.57% with a mean value of $20.44 \pm 9.94\%$ at $E3$ (11.103 keV), 42.62% with a mean value of $30.95 \pm 13.34\%$ at $E4$ (35.83 keV) and 39.17% with a mean value of $22.68 \pm 14.43\%$ at $E6$ (88.6 keV) for Ge-32, Cs-55 and Pb-82, respectively, are presented in Table 2 and shown in

Fig. 1. For the same element, an entirely different set of $A_{\mathrm{MFF+ASF}}(Z, E, v_i^2)$ values as a function of the energy of the incident photon was generated. The results show that $A_{\mathrm{MFF+ASF}}(Z, v_i^2)$ is dependent on the energy of the incident photon. In contrast, $A_{\mathrm{MFF/RFF}}(Z, v_i^2)$ had a single set of values valid for the whole energy range; only the final limit [*i.e.*, $A(Z, E, \bar{v}^2)$] corresponding to the energy of the incident photon changed.

The impact of anomalous scattering effects on Monte Carlo sampling was examined for the coherent scattering of photons by the neutral atoms Ge-32, Cs-55 and Pb-82.

Fig. 2 shows the relative probability density for the scattered photons with energies 1.2167 keV ($E1$), 1.2304 keV ($E2$), 10.966 keV ($E3$) and 11.103 keV ($E4$) (as listed in Table 1) for the neutral atom Ge-32 based on the MFF/RFF and MFF/RFF + ASF schemes. The difference between the curves sampled with the two schemes can be easily seen in the scale of these graphs. A significant increase in forward scattering by the neutral atom Ge-32 was observed for the MFF/RFF + ASF scheme compared to the MFF/RFF scheme for all photon energies studied, as shown in Fig. 2. Fig. 3(*a*) shows a

Muhammad and Lee · Monte Carlo simulation of Rayleigh scattering

comparison of the forward scattering amplitudes calculated by the MFF/RFF and MFF/RFF + ASF schemes. Fig. 3(*b*) shows the % differences between the forward scattering peaks calculated by the MFF and MFF/RFF + ASF schemes for the energies for Ge-32 given in Table 1. A maximum difference of 27.16% was observed for *E*4, which is close to the *K* edge (*i.e.*, 11.1031 keV) for Ge-32, as shown in Fig. 3(*b*).

Fig. 4 shows the relative probability densities based on the MFF/RFF and MFF/RFF + ASF schemes for photons with energies of 5.007 keV (*E*1), 5.301 keV (*E*2), 5.695 keV (*E*3) and 35.83 keV (*E*4) after being scattered by the neutral atom Cs-55. Like Ge-32, an increase in forward scattering by the neutral atom Cs-55 for the MFF/RFF + ASF scheme was observed compared to the MFF/RFF scheme for all the energies studied. Fig. 5 shows a comparison of the forward scattering amplitudes and % differences among the forward scattering peaks calculated by the MFF/RFF and MFF/RFF + ASF schemes for the energies listed for Cs-55 in Table 1. A maximum difference of 32.42% was observed for *E*4 just below the *K* edge (*i.e.*, 35.985 keV) for Cs-55, as shown in Fig. 5(*b*).

Fig. 6 shows the relative probability density based on the MFF/RFF and MFF/RFF + ASF schemes for photons with energies of 2.48 keV (*E*1), 2.58 keV (*E*2), 13.1 keV (*E*3),

15.1 keV (*E*4), 15.6 keV (*E*5) and 88.6 keV (*E*6) (listed in Table 1) after being scattered by the neutral atom Pb-82. A considerable increase in forward scattering was observed in the case of Pb-82, just like in the cases of Ge-32 and Cs-55, for the MFF/RFF + ASF scheme compared to the MFF/RFF scheme for all energies studied, as shown in Fig. 7. In the case of Pb-82, a maximum % difference of 27.6% between the forward scattering peaks calculated by the MFF/RFF and MFF/RFF + ASF schemes was observed at *E*6, slightly above the *K* edge (*i.e.*, 88.0045 keV), as shown in Fig. 7(*b*).

Fig. 8 shows a comparison of the mean % differences [*i.e.*, $A_{\mathrm{mean}}(Z, v_i^2)$] between the normalized values of $A_{\mathrm{MFF/RFF}}(Z, v_i^2)$ and $A_{\mathrm{MFF+ASF}}(Z, v_i^2)$ and the % differences between the forward scattering peaks calculated by the MFF/RFF and MFF/RFF + ASF schemes, respectively, for Ge-32, Cs-55 and Pb-82. From the results, it is concluded that as $A_{\mathrm{mean}}(Z, v_i^2)$ increases, the corresponding % difference between the forward scattering peaks also increases.

The most significant observation that can be extracted from the MC sampling of coherent scattering is the increase in forward scattering due to the inclusion of the ASFs in combination with the MFFs (*i.e.*, the MFF/RFF + ASF scheme) compared to the MFF/RFF scheme. The effect on forward scattering was observed for all three elements and at all energies studied. The maximum increase in forward scattering was witnessed near the *K* edge for all the elements investigated. Along with the maximum effect on the forward scattering amplitudes near the *K* edge, an increase in forward scattering near other edge energies (*i.e.*, L_{I}, L_{II}, L_{III} *etc.*) were also observed for all three elements. However, it is difficult to establish the exact correlation between the increase in the forward scattering amplitude and edge energies due to limitations in defining the boundaries of the edge energies. The results confirmed that the ASFs may be independent of the scattering angle (Kissel *et al.*, 1995) but the angular distribution of the scattered photons is not independent of the ASFs.

The calculated nCDFs for the coherent scattering of photons by the neutral atoms Ge-32, Cs-55 and Pb-82 were plotted against the energy of the incident photons, as shown in Fig. 9. In these graphs, dips are present at the *K*-edge energies for all three elements studied for the MFF/RFF + ASF scheme, while these are absent for the MFF/RFF scheme. Furthermore, the use of the adjective 'anomalous' is fully justified in the calculation of the nCDFs for coherently scattered photons for photon energies around the absorption edges. The results confirmed that for MC sampling of the coherent scattering of photons, the MFF/RFF scheme is approximately valid only for photons with energies well above the *K* absorption edge, while below this energy the MFF/RFF + ASF scheme is useful. In addition, the MFF/RFF scheme for the MC simulation may be useful where coherent scattering is not the primary concern (*i.e.*, simulation of the radiation response function for a detector or when dealing with higher energies of photons). However, when coherent scattering is the primary concern (*i.e.*, when studying the inner structure of atoms/macromolecules/proteins and for other applications of
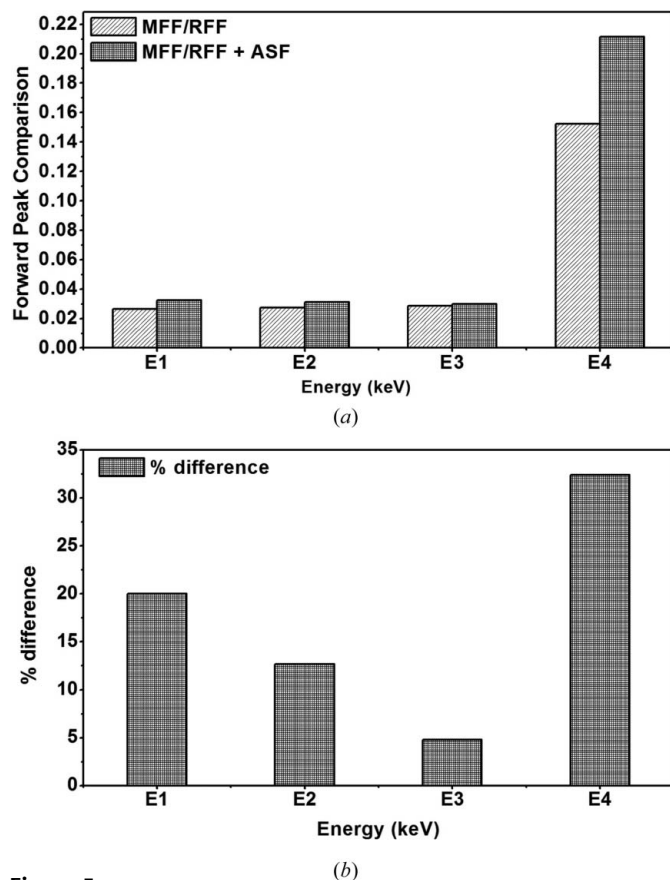

Figure 5
(*a*) Comparison of forward coherent scattering peaks for caesium (Cs, *Z* = 55). (*b*) % difference between the peaks calculated on the basis of the MFF/RFF and MFF/RFF + ASF schemes for caesium. Energies: *E*1 = 5.007 keV, *E*2 = 5.301 keV, *E*3 = 5.695 keV and *E*4 = 35.83 keV.
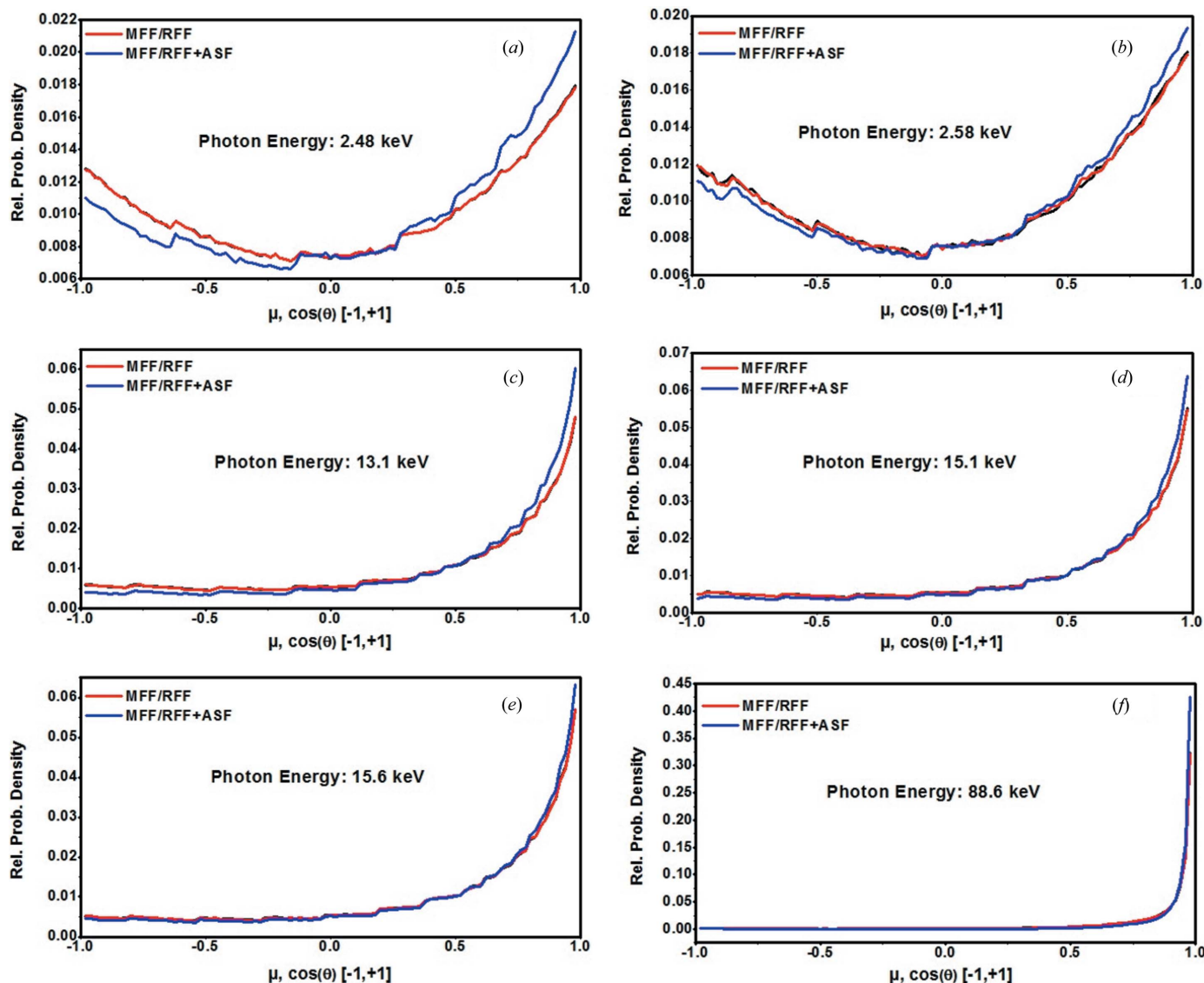
Figure 6
Angular distribution of the coherently scattered photons sampled on the basis of the MFF/RFF and MFF/RFF + ASF schemes for a source of 1 000 000 photons after being scattered by lead (Pb, $Z = 82$) at energies (a) E1 = 2.48 keV, (b) E2 = 2.58 keV, (c) E3 = 13.1 keV, (d) E4 = 15.1 keV, (e) E5 = 15.6 keV and (f) E6 = 88.6 keV.

coherent scattering), better results will be produced with the MFF/RFF + ASF scheme.

Fig. 10(a) shows a comparison of the current MC code results for the RFF and MFF approximation with the experimental and theoretical (i.e., SM, RFF and MFF approximation) data from the literature for the nDCS as a function of the scattering angle for photons with an energy of 59.54 keV after being scattered coherently by the neutral atom tantalum (Ta, $Z = 73$). It shows that the current MC results are close to the corresponding theoretical results for the MFF and RFF approximation, but they do not match either the experimental or SM data. A comparison of the current MC code results for the MFF/RFF + ASF approximation with the experimental and theoretical (i.e. SM, RFF and MFF approximation) data for the nDCS as a function of the scattering angle for photons with an energy of 59.54 keV after being scattered coherently by the neutral atom tantalum, (Ta, $Z = 73$) is shown in Fig.

10(b). The results show that by following the MFF/RFF + ASF approximation, the MC sampling is very close to the corresponding experimental and SM results.

Differentiation of coherent scattering by a complex system and a free/neutral atom is the main source of valuable information on the inner structure of complex systems. The improved MC techniques described here for the sampling of the coherent scattering of photons may be a useful tool for obtaining more precise scientific knowledge. Furthermore, the MFF/RFF + ASF approach can be useful for the MC simulation of coherently scattered photons, producing more accurate coherent amplitudes, which are a useful source of insight, as well as providing assistance in determining the best available predictions efficiently. From the current results and from previous knowledge that ASFs have an important role by creating minima in coherent scattering cross sections just below the photoelectric edges, the role of ASFs in the angular
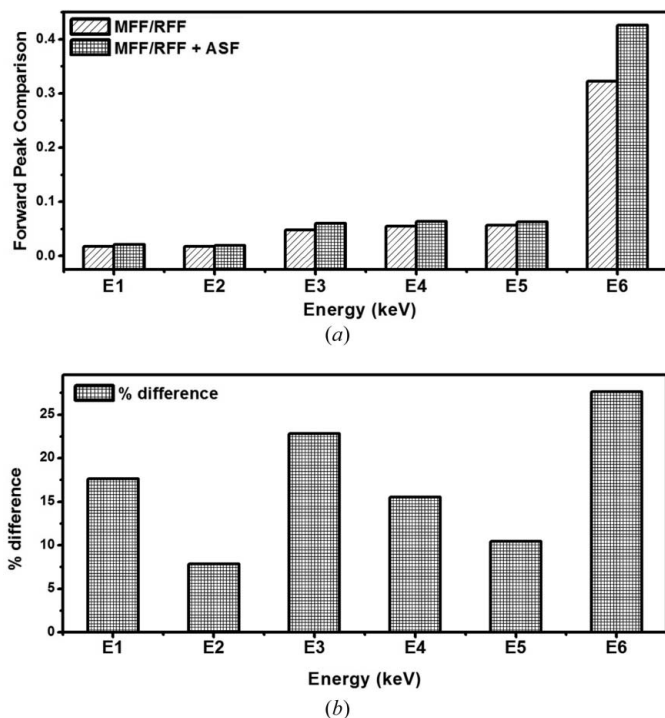
Figure 7
(*a*) Comparison of forward coherent scattering peaks for lead (Pb, Z = 82). (*b*) % difference between the peaks calculated on the basis of the MFF/RFF and MFF/RFF + ASF schemes for lead. Energies: $E1$ = 2.48 keV, $E2$ = 2.58 keV, $E3$ = 13.1 keV, $E4$ = 15.1 keV, $E5$ = 15.6 keV and $E6$ = 88.6 keV.

distribution of coherently scattered photons cannot be ignored. Otherwise, some serious errors in measuring the exact coherent scattering amplitudes, particularly for photon energies around the absorption edges, may result. The use of ASFs in combination with MFFs (*i.e.*, the MFF + ASF scheme) produces an improved and fairly good approximation of the exact scattering amplitudes, particularly within the region around the elemental absorption edges for all three elements investigated in this study.

4. Conclusion

The $A_{\mathrm{MFF+ASF}}(Z, v_i^2)$ values depend upon the energy of the incident photon, while $A_{\mathrm{MFF/RFF}}(Z, v_i^2)$ has a single set of values valid for the whole energy range (*i.e.*, only its final limit is constrained by the energy of the incident photon). The most conclusive observation is the increase in forward scattering due to the inclusion of ASFs in the MC simulation of the coherent scattering of photons by the neutral atoms Ge-32, Cs-55 and Pb-82 for all the energies studied. Although a maximum effect was observed around the K edge, an increase in forward scattering within the regions around the other elemental absorption edges (*i.e.*, L_{I}, L_{II}, L_{III} *etc.*) was also considerable for all three elements. The improved model for MC sampling of coherent scattering has produced an improved and fairly good approximation in excellent agreement with the corresponding experimental and SM results. Furthermore, the current model highlighted the role of ASFs
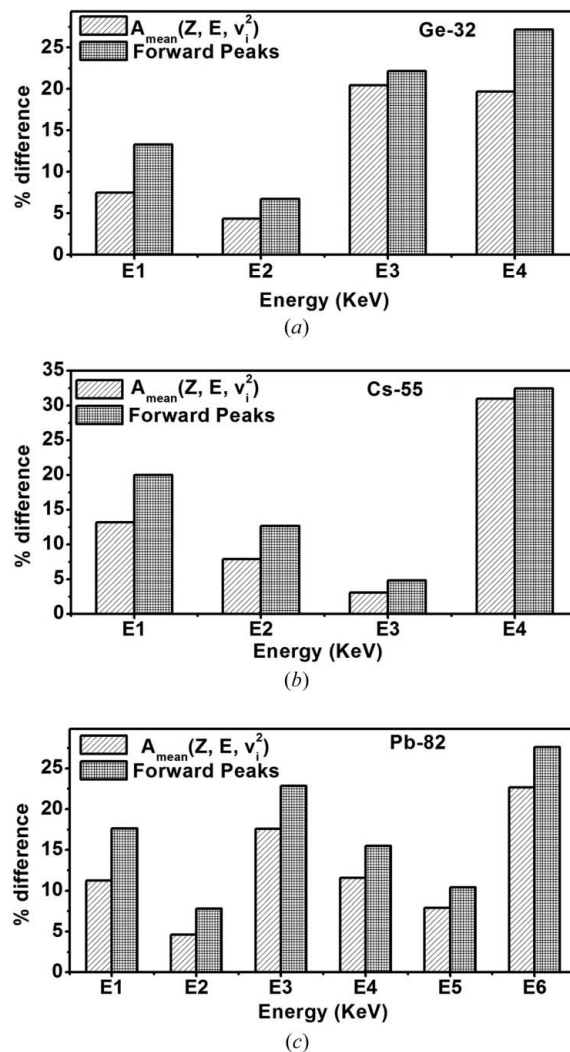

Figure 8
Comparison of the mean % differences between the normalized values of $A_{\mathrm{MFF/RFF}}(Z, v_i^2)$ and $A_{\mathrm{MFF/RFF+ASF}}(Z, v_i^2)$ [*i.e.*, $A_{\mathrm{mean}}(Z, v_i^2)$] and the sampled forward peaks based on the MFF/RFF and MFF/RFF + ASF schemes at the energies listed in Table 1 for (*a*) germanium (Ge, Z = 32) (energies $E1$–$E4$), (*b*) caesium (Cs, Z = 55) (energies $E1$–$E4$) and (*c*) lead (Pb, Z = 82) (energies $E1$–$E6$).

in MC sampling of coherently scatted photons. The current model produced dips in the plots for the nCDFs against the energy of the incident photons at the K-edge energies for all three elements. These dips were absent in the plots produced by the previous MC models (*i.e.*, the MFF/RFF scheme). Some extra scientific information can be obtained with the MFF/RFF + ASF scheme in MC sampling of coherent scattering of photons.
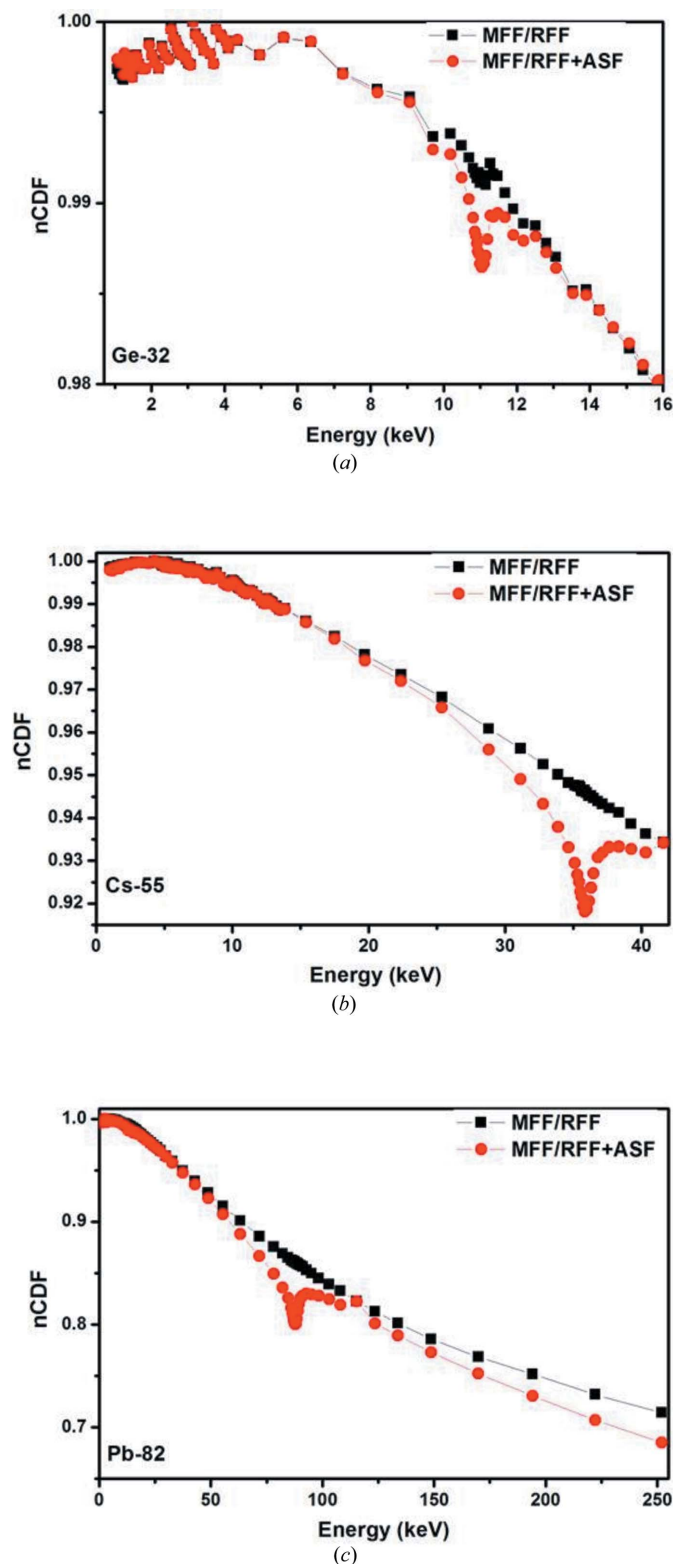
Figure 9
Normalized cumulative probability distribution functions (nCPDFs) of the photon angular distribution, μ, after photons were scattered coherently by neutral atoms of (a) germanium (Ge, $Z = 32$), (b) caesium (Cs, $Z = 55$) and (c) lead (Pb, $Z = 82$) as a function of the energy of the incident photon. The nCPDFs are calculated by numerical integration of the MC sampled angular distribution curves for scattered photons using the MFF/RFF and MFF/RFF + ASF schemes.
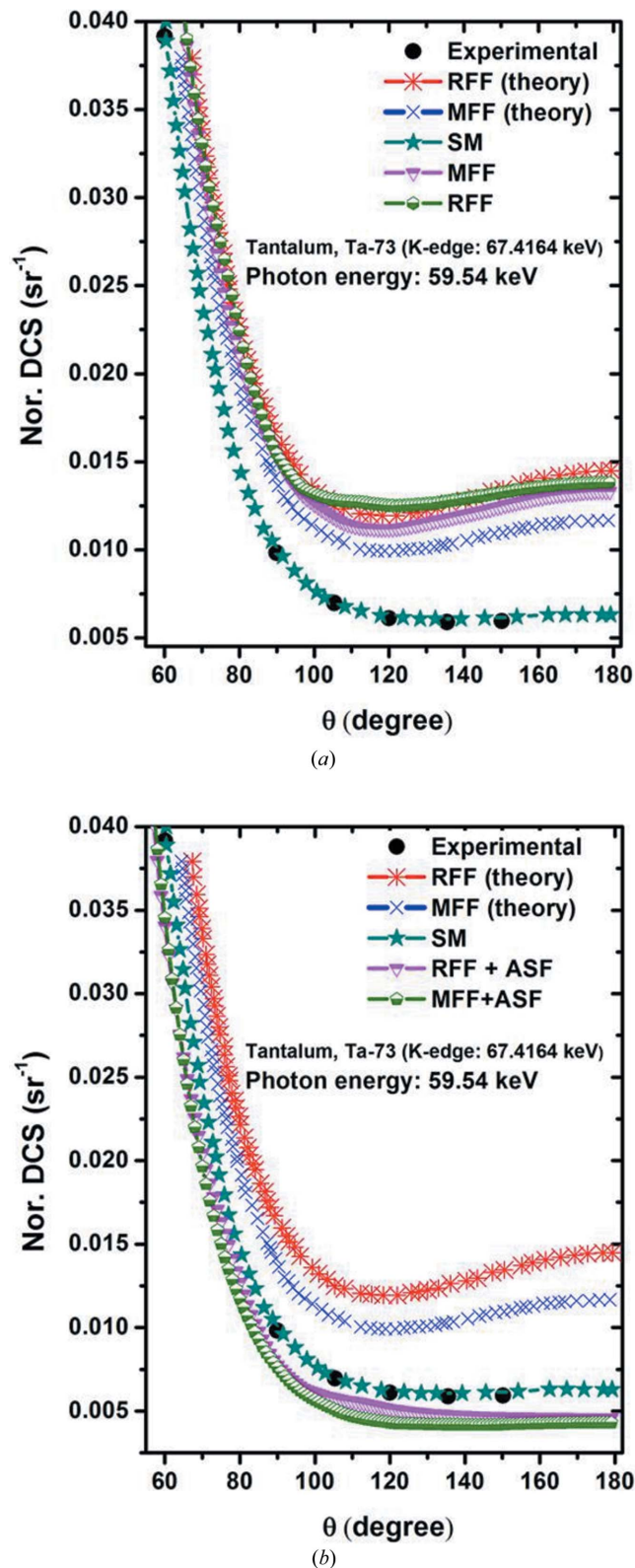

Figure 10
Comparison of experimental and theoretical (*i.e.* SM, RFF and MFF) approximations for the nDCS as a function of scattering angle (θ) from the literature for 59.54 keV photons after being scattered coherently by neutral atoms of tantalum (Ta, $Z = 73$) (Pratt *et al.*, 1993) with the corresponding results from (a) current MC techniques and (b) utilizing the MFF + ASF and RFF + ASF approximations.

research papers

References

Batič, M., Hoff, G., Pia, M. G. & Saracco, P. (2012). *IEEE Trans. Nucl. Sci.* **59**, 1636–1664.

Bergstrom, P. M., Kissel, L., Pratt, R. H. & Costescu, A. (1997). *Acta Cryst.* A**53**, 7–14.

Carter, L. L. & Cashwell, E. D. (1975). Report TID-26607. Los Alamos National Laboratory, Los Alamos, USA.

Chadwick, M. B. *et al.* (2011). *Nucl Data Sheets*, **112**, 2887–2996.

Chantler, C. T. (2000). *J. Phys. Chem. Ref. Data*, **29**, 597.

Cianci, M., Helliwell, J. R., Helliwell, M., Kaucic, V., Logar, N. Z., Mali, G. & Tusar, N. N. (2005). *Crystallogr. Rev.* **11**, 245–335.

Cromer, D. T. (1983). *J. Appl. Cryst.* **16**, 437.

Cromer, D. T. & Liberman, D. (1970). *J. Chem. Phys.* **53**, 1891–1898.

Cullen, D. E. (1989). Report UCRL-ID-103422. Lawrence Livermore National Laboratory, Livermore, USA.

Cullen, D. E. (1995). *Nucl. Instrum. Methods Phys. Res. B*, **101**, 499–510.

Cullen, D. E. (1997). Report UCRL-ID-126455, Rev. 1. Lawrence Livermore National Laboratory, Livermore, USA.

Cullen, D. E. (1998). Report No. UCRL-ID-126455, Rev. 2; DP0102052. Lawrence Livermore National Laboratory, Livermore, USA.

Cullen, D. E. (2000). Report UCRL-ID-126455, Rev. 3. Lawrence Livermore National Laboratory, Livermore, USA.

Cullen, D. E. (2003). Report UCRL-ID-126455, Rev. 4, Part 1. Lawrence Livermore National Laboratory, Livermore, USA.

Cullen, D. E. (2012). Personal communication.

Cullen, D. E., Hubbell, J. H. & Kissel, L. (1997). *EPDL97: The Evaluated Photon Data Library, '97 Version*. http://www-nds.iaea.org/epdl97/document/epdl97.pdf.

Demarco, J. J., Wallace, R. E. & Boedeker, K. (2002). *Phys. Med. Biol.* **47**, 1321–1332.

Henke, B., Gullikson, E. & Davis, J. (1993). *At. Data Nucl. Data Tables*, **54**, 181–342.

Henke, B. L., Lee, P., Tanaka, T. J., Shuimabukuro, R. L. & Fujikawa, B. K. (1981). *AIP Conf. Proc.* **75**, 340.

Hubbell, J. H. & Overbo, I. (1979). *J. Phys. Chem. Ref. Data*, **8**, 69.

Hubbell, J. H., Veigele, W. J., Briggs, E. A., Brown, R. T., Cromer, D. T. & Howerton, R. J. (1975). *J. Phys. Chem. Ref. Data*, Vol. 4, No. 3, pp. 471–538.

Kane, P., Kissel, L., Pratt, R. & Roy, S. (1986). *Phys. Rep.* **140**, 75–159.

Kawrakow, I. M.-H., Rogers, E. D. W. O., Tessier, F., Walters, B. R. B. & Rogers, D. (2010). *The EGSnrc Code System*. NRCC Report PIRS-701. National Research Council Canada, Ottawa, Canada.

Kissel, L. (2000). *Radiat. Phys. Chem.* **59**, 185–200.

Kissel, L., Zhou, B., Roy, S. C., Sen Gupta, S. K. & Pratt, R. H. (1995). *Acta Cryst.* A**51**, 271–288.

Muhammad, W. & Lee, S. H. (2013). *J. Radiat. Res.* **54**, 190–201.

Persliden, J. (1983). *Comput. Programs Biomed.* **17**, 115–128.

Pratt, R. H., Bergstrom, P. M. J. & Kissel, L. (1993). *New relativistic S-matrix results for scattering – beyond the usual anomalous factors/ beyond impulse approximation*. Report No. UCRL-JC–114583; CONF-9208186–5. Lawrence Livermore National Laboratory, Livermore, USA.

Roy, S., Kissel, L. & Pratt, R. (1999). *Radiat. Phys. Chem.* **56**, 3–26.

Roy, S., Pratt, R. & Kissel, L. (1993). *Radiat. Phys. Chem.* **41**, 725–738.

Salvat, F., Fernández-Varea, J. M. & Sempau, J. (2011). *PENELOPE*. http://www.oecd-nea.org/dbprog/courses/peneloperef.html.

Schaupp, D., Schumacher, M., Smend, F., Rullhusen, P. & Hubbell, J. H. (1983). *J. Phys. Chem. Ref. Data*, **12**, 467.

Sultana, A., Reznik, A., Karim, K. S. & Rowlands, J. A. (2008). *IEEE Semiconductor Conference, 2008. CAS 2008. International*, Vol. 1, 193–196.

Tartari, A., Taibi, A., Bonifazz, C. & Baraldi, C. (2002). *Phys. Med. Biol.* **47**, 163–175.

X-5 Monte Carlo Team (2003). *MCNP – A General Monte Carlo N-Particle (MCNP) Transport Code, Version 5*. Vol II. *User's Guide*. Report LA-CP-03-0245. http://mcnp.lanl.gov/.